Acta Materialia 161 (2018) 12–20

Contents lists available at ScienceDirect

Acta Materialia

journal homepage: www.elsevier.com/locate/actamat

# Cluster hardening in Al-3Mg triggered by small Cu additions

S. Medrano [a, *], H. Zhao [b], F. De Geuser [c], B. Gault [b], L.T. Stephenson [b], A. Deschamps [c], D. Ponge [b], D. Raabe [b], C.W. Sinclair [a]

[a] Department of Materials Engineering, The University of British Columbia, Stores Road, 309-6350, Vancouver, Canada
[b] Max-Planck-Institut für Eisenforschung, Max-Planck-Str. 1, 40237 Düsseldorf, Germany
[c] Univ. Grenoble Alpes, CNRS, Grenoble INP, SIMAP, Grenoble, 38000, France

ARTICLE INFO

*Article history:*
Received 16 February 2018
Received in revised form
11 June 2018
Accepted 26 August 2018
Available online 30 August 2018

*Keywords:*
Precipitation
Aluminum alloys
Yield strength
Atom probe

ABSTRACT

The aging response of two Al-3Mg alloys with Cu addition < 1 wt% has been tracked under simulated automotive paint bake conditions (~ 20 min, 160 and 200 °C) to quantify the processes controlling hardening. The decomposition of the solid solution, observed by atom probe tomography, has been interpreted using a novel pair correlation function approach and incorporated into a model for prediction of precipitation hardening. It is shown that the hardening is controlled by clusters/Guinier-Preston-Bagaryatsky (GPB) zones similarly to what has been previously observed in much higher Cu containing 2XXX-series alloys. Interestingly, it is shown that very small additions of Cu ( < 0.1 at%) can be used to catalyze a high number density of strengthening particles owing to the high enrichment in Mg compared to particles found in more conventional high Cu/low Mg alloys. This allows hardening during the first hour of aging that is as high as that obtainable in these high Cu alloys.



## 1. Introduction

There is evidence that additions of less than 0.5 at%Cu to 5XXX-series aluminum alloys can counterbalance the softening experienced by stamped then 'paint baked' (~ 150–200 °C for ~ 20 min) automotive aluminum components [1–3]. Being able to retain the as-stamped strength in this way facilitates both reduced material usage and adoption of lower grade Cu-residual scrap in primary alloy production [4]. Finding the minimum Cu content to achieve this is essential to ensure that the weldability and work hardening capacity of the 5XXX alloy can be preserved.

Knowing how to choose the correct minimum level of Cu in this case requires an understanding of the microstructural changes and correlated mechanical response. To date, few studies of this kind have been performed for the low (≲ 1 wt%) Cu Al-Mg alloys [3,5–8]. In contrast, many studies have been published on the related high (≳ 1 wt%) Cu and low (≲ 2 wt%) Mg 2XXX series Al-Cu-Mg alloys [9–14]. These precipitation hardenable alloys undergo a complex precipitation sequence, from random solid solution to solute clusters, GPB zones, S" phase and finally S'/S phase(s) (see e.g. Ref. [15].

Both 2XXX-series alloys [16,17] and Cu modified 5XXX-series alloys [7] exhibit a rapid increase in yield strength in the first few seconds of aging at temperatures between 150 and 200 °C. In 2XXX-series alloys this has been linked to the formation of solute clusters and GPB zones [16,17]. No similar experimental link has been made between precipitate phases and yield strength in the case of the low Cu/high Mg alloys [7,18].

One of the challenges in both alloy classes is our poor understanding of the structure, composition and density of solute clusters/GPB zones existing at short aging times. While the structural model proposed by Kovarik et al. [19] was shown to be consistent with some of the experimentally observed characteristics of clusters/GPB zones [18,20], it does not predict the composition of solute clusters/GPB zones measured by atom probe tomography in model [16], or commercial Al-Cu-Mg alloys [15]. Moreover, much of the available experimental work on the structure and chemistry of these phases focuses on results obtained after long aging times (several hours) where characterization is notably easier [5,18–20]. The relevance of such long term aging observations to the specific microstructure-hardening response in the paint bake cycle remains uncertain.

The aim of this work is to correlate precipitation to yield strength in Cu-modified Al-3Mg alloys at times and temperatures relevant to the industrial automotive paint bake cycle, emphasizing the effect of additions of < 0.5 at%Cu on the yield strength

* Corresponding author.
*E-mail address:* sebastian.medrano@alumni.ubc.ca (S. Medrano).

https://doi.org/10.1016/j.actamat.2018.08.050
1359-6454/

evolution. The evolution of the tensile mechanical properties and electrical resistivity are followed during aging at 160 °C and 200 °C for times of up to 7 h. To overcome the challenges of characterizing precipitates with low atomic number contrast (this limiting techniques such as STEM and SAXS), atom probe tomography has been used for characterization. A parameter free pair-correlation based technique has been used to identify the presence of clusters/particles and a model used to interpret their size and composition. These results are subsequently fed to a precipitation hardening model to predict the experimentally measured hardening response.

## 2. Materials and experimental method

Two laboratory cast and hot rolled 5 mm sheets were provided for this study by the Novelis Global Technology Centre (see Table 1). This material was cold rolled to a thickness of 1 mm (80% reduction in thickness). Tensile samples were cut and solution treated at 550 °C for 10 min, then quenched immediately in water. These were then artificially aged in an oil bath at 160 °C or 200 °C for up to 7 h. All uniaxial tensile tests were performed at 77 K, with an initial nominal strain rate of $10^{-3}$ $s^{-1}$. These conditions were selected so as to avoid the complicating effects of dynamic strain aging [21]. Resistivity measurements were also performed in a liquid nitrogen bath at 77 K using a four-point probe with an applied current of approximately 20 mA and a reversion frequency of 30 Hz [22].

Specimens for APT were prepared by solution treating and artificially aging sheet material, following the procedure described above. Samples were cut following aging and turned into needle-shaped specimens using a conventional 2-stage electrochemical polishing technique employing perchloric acid [23]. Atom probe data was acquired on a Cameca LEAP 5000 XS at a base temperature of 50 K, in high-voltage pulsing mode, with 20% pulse fraction, with the DC voltage adjusted to maintain a detection rate of 1 ion per 100 pulses. Data reconstruction was performed in the commercial software package IVAS 3.6.14, and using the calibration methods outlined in Refs. [24,25]. Precipitates were visualized by means of isocomposition surfaces [26] and composition of individual object by composition profiles derived from the regions-of-interest.

## 3. Experimental characterization of aging response

The tensile response of the 0.23 at%Cu alloy aged at 200 °C (Fig. 1) shows that its yield strength rises rapidly from 87 MPa to 150 MPa within the first 2 min. This is followed by a gradual but continuous increase of the yield strength over the following 18 h (1100 min). Aside from the evolution of the yield strength, no other changes in the stress-strain response were noted. The lack of change in work hardening rate (Fig. 1(b)) is particularly notable as it suggests that the hardening phase(s) are predominantly small and shearable (see e.g. Ref. [21]). The second factor that might be expected to effect the work hardening rate (via dynamic recovery [27]) is the change of solute in solid solution. As will be shown shortly, the amount of solute removed from solid solution during aging is too small to have a noticable effect on the work hardening rate (cf. Tables 2 and 3). This result mirrors the behaviour observed for all other aging conditions tested.

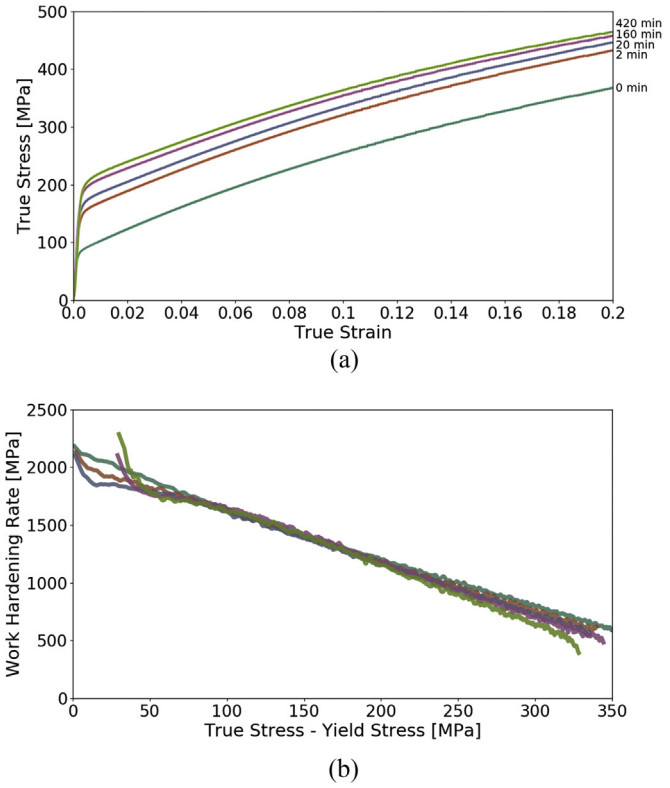


**Fig. 1.** a) The tensile true stress-true strain response for the alloy containing 0.23 at.% Cu in the solid solution state (0 min of aging), after 2 min, 20 min, 160 min and 420 min aging at 200 °C. b) The same data as in (a) but plotted as a Kocks-Mecking plot showing the collapse of the work hardening rates when the yield strength is subtracted from the flow stress.

Fig. 2 presents the 0.2% offset yield strength evolution for the two alloys aged at 200 °C and the 0.23 at.%Cu alloy aged at 160 °C. Interestingly, the yield strength is seen to evolve at a similar rate for all conditions beyond the first 2 min of aging. This matches the linear evolution of yield strength with logarithmic time reported by Court and Lloyd [1] on similar alloys tested at room temperature after aging. Moreover, the similarity of the aging response of the 0.23 at.%Cu alloy at 160 and 200 °C agrees with the results presented for similar alloys by Ratchev et al. [2]. Comparing the behaviour of the 0.12 and 0.23 wt%Cu alloys, it is impressive that alloy containing ~50% less Cu is able to provide 75% of the strength of the 0.23 at.%Cu alloy.

Electrical resistivity has been widely used as a mean-field characterization technique in cluster and precipitation hardening aluminum alloys [28–30]. Changes in resistivity reflect both the loss of solute from solid solution and, in the case of sufficiently fine clusters/precipitates, an increase in scattering arising from phase interfaces. While disentangling the effects of solid solution and interfaces in these alloys can be challenging [31], the method gives an independent measurement for comparison against the tensile data and more local microstructural information obtained from APT or (S)TEM.

**Table 1**
Composition obtained by OES of alloys studied. Balance is aluminum.

| | | Mg | Cu | Fe | Si | Ti | Ni | Mn | Zn | Cr |
|---|---|---|---|---|---|---|---|---|---|---|
| 0.23 at.%Cu Alloy | (at.%) | 3.23 | 0.229 | 0.048 | 0.048 | 0.008 | 0.003 | 0.0005 | 0.00008 | 0.0005 |
| | (wt.%) | 2.90 | 0.54 | 0.1 | 0.05 | 0.015 | 0.007 | 0.001 | 0.002 | 0.001 |
| 0.12 at.%Cu Alloy | (at.%) | 3.20 | 0.115 | 0.046 | 0.046 | 0.007 | 0.003 | 0.0005 | 0.0012 | 0.0005 |
| | (wt.%) | 2.96 | 0.28 | 0.1 | 0.05 | 0.014 | 0.007 | 0.001 | 0.003 | 0.001 |

**Table 2**
The mean particle size ($\langle R \rangle$) and standard deviation ($S$) of assumed log-normal particle size distribution, volume fraction ($f_v$), number density and composition of particles obtained by fitting to the data in Fig. 5 assuming two log-normal particle size distributions in each aging condition. The Al content was fixed at 80 at% based on the composition profiles extracted in Fig. 4.

| Aging Time | Particle | $\langle R \rangle$ | $S$ | $f_v$ | $N_v$ | Al (at%) | Cu (at%) | Mg (at%) |
|---|---|---|---|---|---|---|---|---|
| 20 min | Cu Lean Particles | 0.73 nm | 0.48 | 0.23% | $4.9 \times 10^{23}$ m$^{-3}$ | 80 | 1 | 19 |
| | Cu Rich Particles | 2.2 nm | 0.4 | 0.16% | $1.8 \times 10^{22}$ m$^{-3}$ | 80 | 5 | 15 |
| 160 min | Cu Lean Particles | 2.4 nm | 0.16 | 0.23% | $3.6 \times 10^{22}$ m$^{-3}$ | 80 | 2 | 18 |
| | Cu Rich Particles | 3.2 nm | 0.4 | 0.17% | $6.3 \times 10^{21}$ m$^{-3}$ | 80 | 7 | 13 |

**Table 3**
Parameters used/calculated in predicting the yield strength of the alloy after aging for 20 min and 160 min at 200 °C. The relative strengths of the particles ($\beta = F_m/2\Gamma$) are also reported.

| Aging Time at 200°C | $\sigma_0$ (MPa) | $\sigma_{ss-Cu}$ (MPa) | $\sigma_{ss-Mg}$ (MPa) | $r_c$ (nm) | $\sigma_{ppt}$ (MPa) (Cu Rich) | $\beta$ (Cu Rich) | $\sigma_{ppt}$ (MPa) (Cu Lean) | $\beta$ (Cu Lean) | $\sigma_{ys}$ (MPa) Predicted | $\sigma_{ys}$ (MPa) Experimental |
|---|---|---|---|---|---|---|---|---|---|---|
| 20 min | 20 | 30 | 58 | 3.95 | 104 | 0.5 | 87 | 0.2 | 170 | 170 |
| 160 min | 20 | 29 | 58 | 3.95 | 106 | 0.7 | 124 | 0.5 | 195 | 196 |

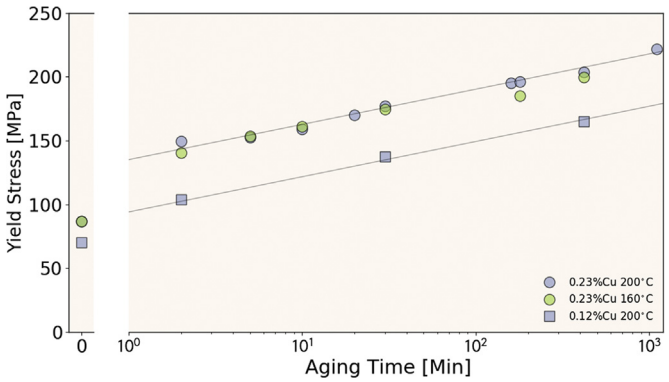


**Fig. 2.** The evolution of the 0.2% offset yield strength for the 0.23 at.%Cu alloy aged at 160 and 200 °C and the 0.12 at.%Cu alloy at 200 °C for times ranging from 2 min to 1100 min. The yield strength of the solution treated sample is shown on the far left side of the plot. Lines are drawn as a guide to the eye.

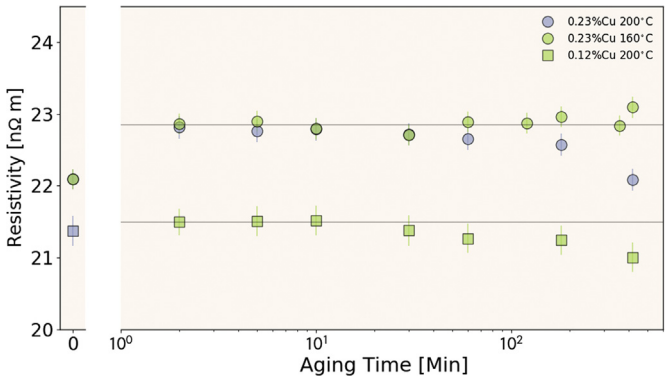


**Fig. 3.** The time evolution of electrical resistivity for the 0.23 at%Cu alloy at 200 °C and 160 °C and the 0.12 at.%Cu alloy aged at 200 °C for the same aging times used to produce Fig. 2. The resistivity of the solution treated samples is shown on the far left. Error, shown as the bars on each data point, was calculated based on the uncertainty in measured resistance and area. The lines are shown as a guide to the eye.

Fig. 3 shows the change in electrical resistivity for those samples whose yield strength is shown in Fig. 2. The higher as-quenched resistivity for the 0.23 at.%Cu alloy compared to the 0.12 at.%Cu alloy reflects the higher overall solute content. Consistent with the 'rapid hardening' behaviour illustrated in Fig. 2, the resistivity also increases rapidly within the first 2 min of aging, the magnitude of the jump being much larger in the case of the 0.23 at.%Cu alloy compared to the 0.12 at.%Cu alloy. This rapid increase is consistent with the formation of small solute clusters that contribute significantly to conduction electron scattering (cf. results on 2XXX-series alloys [32,33]). Following the rapid initial resistivity jump, both alloys exhibit a long period ( > 100 min) of nearly constant resistivity followed by a slow decrease for the 200 °C samples. It is notable that the resistivity evolution of the 0.23 at.%Cu alloy aged at 160 and 200 °C are nearly identical. This observation matches the nearly identical yield strength response shown in Fig. 2.

To investigate the microscopic origin of the observed changes in yield strength and resistivity, atom probe tomography was performed on samples taken from the 0.23 at. %Cu alloy after aging at 200 °C for 20 min (typical paint bake time) and 160 min of aging (end of the resistivity plateau in Fig. 3). Ideally, one would like to compliment such local observations with other cluster/GPB zone sensitive techniques such as HR-TEM, STEM and/or SAXS/SANS to provide better statistics to these observations. As pointed out earlier, however, the lack of atomic number contrast in these alloys drastically limits the options for complimentary techniques. This has, in our opinion, been the major stumbling block for previous studies on the early stages of aging in this alloy system. Fig. 4(a) shows an APT volume measured on a sample aged for 20 min. Within this volume iso-surfaces reveal a distribution of small Mg and Cu enriched particles. The one-dimensional composition plots for the selected particles reveal the particles to contain approximately 80–90 at.%Al, 10–15 at.%Mg and 1–5 at.%Cu. Further aging to 160 min (Fig. 4(b)) led to only minor changes in the composition and sizes of the particles based on iso-surface and one-dimensional composition plots. In both cases, the compositions were found to be similar to, but distinct from, those previously reported for clusters/GPB zones in an AA2024 alloy (4.3 wt%Cu, 1.3 wt%Mg) [15].

Relying on conventional cluster finding algorithms has drawbacks owing to the underlying assumptions that one must make [34]. Cluster-finding methods are usually prone to parameter-selection biases [35] in particular for cases where multiple morphologies of features are present [36]. As an alternative method, a pair correlation based approach has been adopted here to interpret the results in Fig. 4. This radial distribution function based method for extracting information on clusters and precipitates [37], and its direct relationship to the formalism conventionally used in small

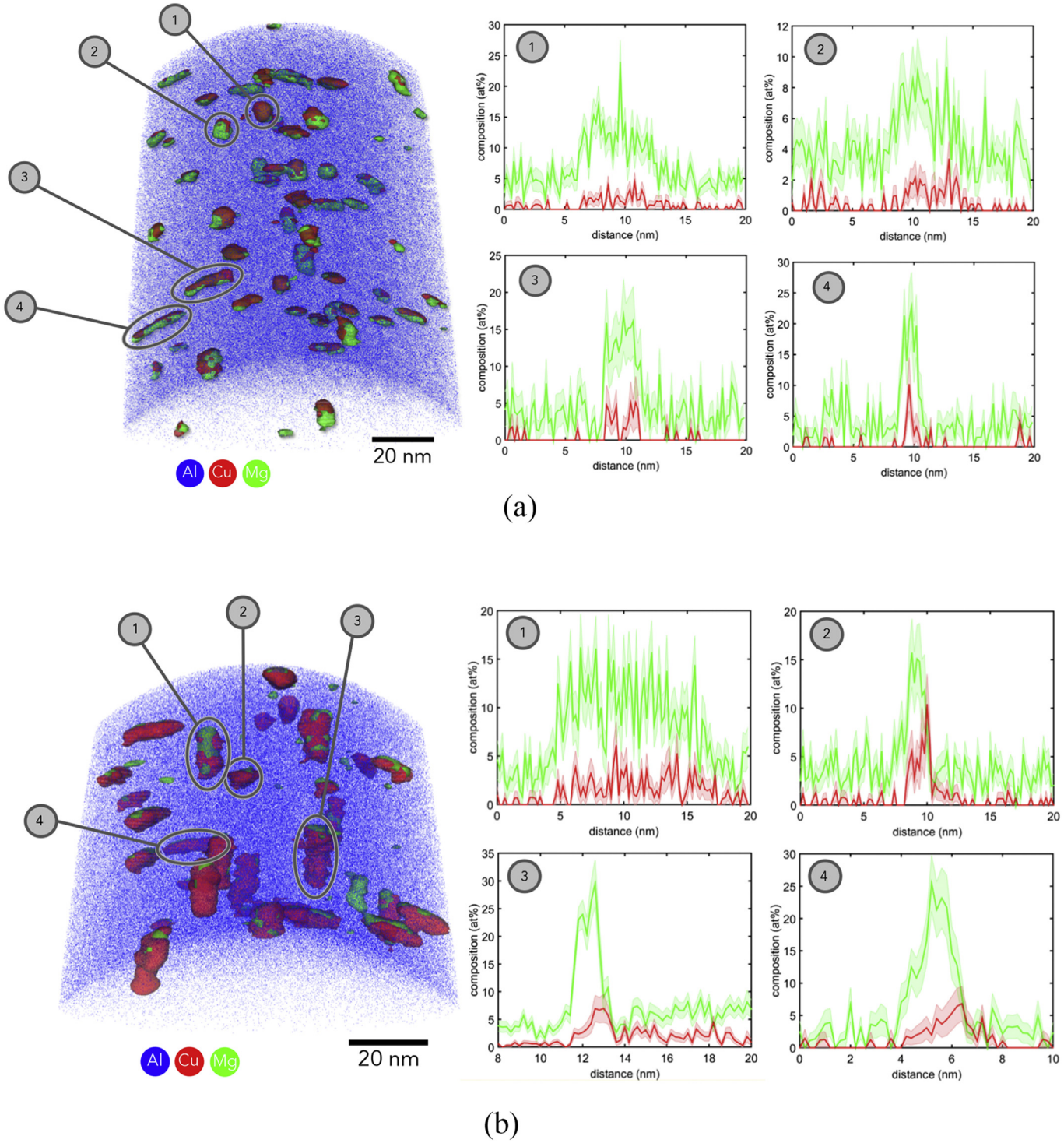


**Fig. 4.** Atom probe volumes measured on samples aged for a) 20 min and b) 160 min at 200 °C. In each case, iso-surfaces corresponding to a) 3.13 atoms/nm$^3$ Mg and 0.5 atoms/nm$^3$, and b) 3.5 atoms/nm$^3$ Mg 1.0 atoms/nm$^3$ Cu are plotted to reveal the presence of small Mg and Cu rich particles. One dimensional composition plots are provided along two perpendicular directions, the results being representative of the observations made in the other particles.

angle scattering, has been established [38,39] and used recently for studying clustering in aluminum alloys by Ivanov et al. [40]. The pair correlation approach used here has the advantage of providing a self-consistent, parameter free description of the solute distribution within the dataset. This can then be interpreted to obtain information on particle size and composition when combined with a suitable model.

We use a modified definition of the pair correlation function (PCF) compared to the one introduced in Ref. [41]. The form used here allows the PCF to be expressed in an equivalent way to the form used in small angle scattering in the case of an isotropic two-phase system where the composition is uniform within the two phases [38,40,42,43]. We define a pair correlation function as,

$$\gamma_{i-j}(r) = c_0^i c_{i-j}(r) - c_0^i c_0^j \quad (1)$$

where $c_0^j$ is the average concentration of species $j$ in the alloy and $c_{i-j}(r)$ is the concentration of species $j$ at a distance $r$ from an atom of species $i$ averaged over all atoms of species $i$. $\gamma_{i-j}(r)$ is the correlation between the concentration fluctuations in element $i$ and element $j$, i.e. $\langle \Delta c^i \Delta c^j \rangle$. Equation (1) can be written in terms of two contributions,

$$\gamma_{i-j}(r) = \gamma_{ij}(0)\gamma_0(r) \quad (2)$$

The function $\gamma_0(r)$ is a normalized correlation function, such that $\gamma_0(0) = 1$ and $\gamma_0(r \to \infty) = 0$. The meaning of $\gamma_0(r)$ is particularly intuitive in the case of a single object in a (infinitely) large homogeneous volume. In this case $\gamma_0(r)$ is the normalized autocorrelation; it is the intersection volume of the object and its 'ghost' displaced by a distance $r$ normalized by the object volume. For simple shapes, this function can be determined analytically. For example, for spherical particles of radius $R$, $\gamma_0(r)$ is [44],

$$\gamma_0^{sphere}(r) = \begin{cases} 1 - \dfrac{3r}{4R} + \dfrac{r^3}{16R^3} (r \le 2R) \\ 0 (r > 2R) \end{cases} \quad (3)$$

In the case of randomly distributed precipitates whose radii are distributed (e.g. following a log-normal distribution) a volume weighted numerical integration of Equation (3) can be performed to obtain $\gamma_0(r)$.

It is important to note that $\gamma_0(r)$ is a unique function of the size and geometry of the second phase. The effect of matrix/particle composition enters entirely through $\gamma_{i-j}(0)$ which is a measure of the compositional contrast between the phases. In the case of the correlation between atoms of the same type,

$$\gamma_{i-i}(0) = f_v(1 - f_v)\left(c_p^i - c_m^i\right)^2 \quad (4)$$

while in the case of the correlation between two different types of atoms we obtain,

$$\gamma_{i-j}(0) = f_v(1 - f_v)\left(c_p^i - c_m^i\right)\left(c_p^j - c_m^j\right) \quad (5)$$

In the above equations, $c_p$ and $c_m$ refer to the particle and matrix compositions, $c_0$ to the average compositions and $f_v$ to the volume fraction of particles. It is important to note that for a pseudo-binary situation, i.e. if only one type of objects are present, the 3 PCFs $\gamma_{i-i}(r), \gamma_{j-j}(r)$ and $\gamma_{i-j}(r)$ should all be proportional, the factor of proportionality being related to the fraction of objects and the composition contrast. Moreover, based on the definitions given above,

$$\gamma_{i-j}(0) = \sqrt{\gamma_{i-i}(0)\gamma_{j-j}(0)} \quad (6)$$

In the present case, we have calculated the Mg-Mg, Cu-Cu and Mg-Cu pair correlations (Fig. 5) from the APT data shown in Fig. 4. If the particles observed in Fig. 4 belonged to a single population with a uniform composition, then all three pair correlation functions should be proportional to one another. Careful observation of the Mg-Mg and Cu-Cu pair correlations shows that this can't be true as the correlation length for the Cu-Cu pair correlations is noticeably longer than that for the Mg-Mg pair correlations.

The results in Fig. 5 can be interpreted in terms of particle/matrix compositions and particle sizes if a model for the phases is proposed. Here, it has been assumed that the particles in the APT volumes are spherical, the radii of the particles following a log-normal size distribution. Analysis of the iso-contour data in Fig. 5 suggests that the aspect ratio of the particles increases on aging from ~1 at 20 min to close to 2 at 160 min of aging. We have, nevertheless, retained the assumption of spherical particles so as to keep the number of fitting parameters as small as possible. Moreover, the effect of this approximation on the prediction of yield strength based on particle size presented below, is expected to be nearly insensitive to this assumption for such small aspect ratios [45].

To account for the fact that the pair correlations in Fig. 5 do not scale with one another, we have considered that two populations of particles exist, one being richer in Cu with a larger correlation length compared to the other. From fitting $\gamma_{Mg-Mg}(0)$, $\gamma_{Cu-Cu}(0)$

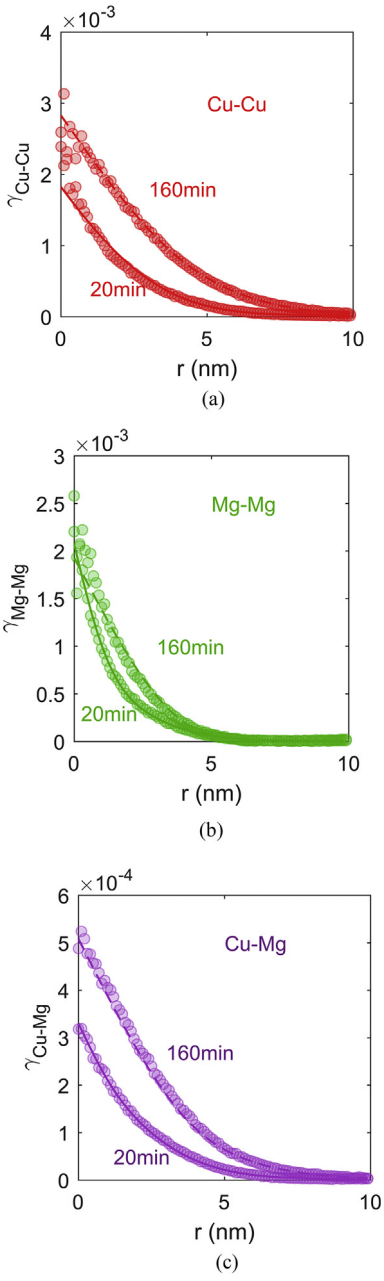


**Fig. 5.** Experimental (symbols) and fit (coloured lines) pair correlation functions for a) Cu-Cu pairs, b) Mg-Mg pairs and c) Mg-Cu pairs from the APT datasets shown in Fig. 4. If all particles belonged to the same population having a uniform composition, then the three figures should simply scale with one another.

and $\gamma_{Cu-Mg}(0)$ one would like to be able to independently obtain the particle compositions and volume fractions (for the assumed two particle types) as well as the matrix composition. In order to do this one extra piece of information needs to be supplied. In the present case we have assumed that the particles contained 80 at% Al based on the profiles in Fig. 4.

Under the above assumptions it was possible to obtain two size distributions and particle compositions from the APT volumes (Fig. 6). The resulting fits to the pair correlations are shown as solid, coloured, lines superimposed on the experimentally determined pair correlations (symbols) in Fig. 5. The values obtained from the fit are also given in Table 2. Consistent with the composition profiles shown in Fig. 4, the particles are seen to be systematically richer in Mg than Cu, with the Cu:Mg ratio being highest in the largest precipitates. With increased aging time, both distributions are seen to shift to larger particle sizes, again qualitatively consistent with the results from the isocomposition plots (Fig. 4). Interestingly, the volume fractions of the two populations are observed to remain constant, suggesting a process of coarsening rather than growth. This interpretation would also be consistent with our resistivity results (Fig. 3) when interpreted using resistivity models [46,47] that predict cluster contributions to the resistivity proportional to volume fraction, and provide also an explanation for the resistivity decrease at long aging times observed at 200 °C, likely due to the coarsening of the particle distribution.

## 4. Predicting yield strength evolution from microstructural observations

If the features seen in APT (Fig. 4) are responsible for the evolution in yield strength reported in Fig. 2 it should be possible to use the data from Fig. 6 to predict the evolution of yield strength with time. Calculating the strength of such a distribution of precipitates must be done carefully as the way in which one chooses to calculate the average strength of such an assembly can have a strong influence on the prediction [21,48]. Here, for simplicity, We take a slightly modified approach to the one originally proposed by Deschamps et al. [49] where the average strength of a distribution of obstacles is calculated as the average of the individual obstacle strengths [21]. It has been shown, by comparing to the results of areal glide simulations, that this approach provides a lower limit estimate to the strength of a distribution of obstacles, the predictions being better for narrower and weaker obstacle populations [48].

We start by assuming that the strength of an individual particle is proportional to the radius of the circle ($r$) formed by the intersection of the spherical particle and the glide plane [50]. The distribution of circle radii ($f(r)$) formed by cutting the spherical particles (having a distribution of radii $g(R)$, where $R$ is the sphere radius) can be calculated from Wicksell's fundamental integral equation [50,51],

$$f(r) = \frac{r}{\overline{R}} \int_0^\infty \frac{g(R)dR}{\sqrt{R^2 - r^2}} \tag{7}$$

where $\overline{R}$ is the mean value of the sphere radii.

The contribution of the precipitates to the macroscopic yield stress is defined as,

$$\sigma_{ppt} = M \frac{Gb}{\overline{L_s}} \overline{\tau^*} \tag{8}$$

where $M$ is the Taylor factor, $G$ is the shear modulus of aluminum and $b$ is the magnitude of the Burgers vector. The average square spacing of precipitates in the glide plane, $\overline{L_s}$, is taken following Ardell [52] as,

$$\overline{L_s} = \left(\frac{2\pi}{3f}\right)^{1/2} \overline{R} \tag{9}$$

The normalized average strength of the ensemble of particles, $\overline{\tau^*}$ is calculated as,

$$\overline{\tau^*} = \int_0^\infty \tau(r)^* f(r) dr \tag{10}$$

In this expression, $\overline{\tau^*}$ is the strength of a randomly distributed population of particles whose size in the glide plane is $r$. In the approach originally proposed by Ref. [49] the strength of obstacles was assumed to obey Friedel's law, this only being strictly valid in the limit of weak obstacles. This approach was generalized by Ref. [21] to include obstacles of all strengths by using the classic result of Foreman and Makin [53] Here, we take the same approach, but use an updated relationship between obstacle strength and particle size arising from computer simulations [54],

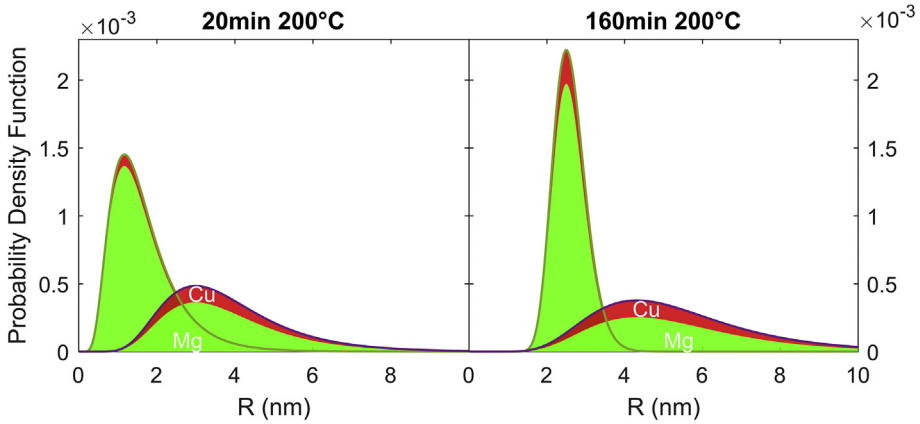


**Fig. 6.** The best fit log-normal size distributions corresponding to the pair correlations shown in Fig. 5. Left: aging for 20 min at 200 °C. Right: aging for 160 min at 200 °C. The green and red areas account for the respective amounts of Cu and Mg in the particles. The results are given as a volume weighted distribution, or $\frac{df}{dR}$. (For interpretation of the references to colour in this figure legend, the reader is referred to the Web version of this article.)

$$\tau(r)^* = \begin{cases} 0.9\left(\frac{r}{r_c}\right)^{3/2}\left(1-\frac{1}{6}\left(\frac{r}{r_c}\right)^5\right) \text{ if } r < r_c \\ 0.75 \text{ if } r \geq r_c \end{cases} \quad (11)$$

The parameter $r_c$ in this expression is the critical size at which the particles transition from being shearable to non-shearable. It was noted, in relation to Fig. 1, that the lack of change in work hardening indicates the presence of shearable particles. When considering a distribution of particle sizes one must, however, consider the possibility of sizes that span a range of sizes from below to above $r_c$.

The presence of two particle distributions (one lower in Cu, the other higher in Cu) leads to a question of whether one should use different $r_c$ for each distribution. It has been argued, though not proved definitively, that precipitation/cluster hardening in Al-Cu-Mg alloys is sensitive to the composition of the phases present [16]. Here, we have chosen to fix a single value of $r_c$ so as to minimize the number of adjustable parameters. Even with a single value of $r_c$, the two particle distributions (Fig. 6) lead to two values of $\sigma_{ppt}$ according to Equation (8). Considering that the strengths and densities of these two particle distributions will be similar, the most appropriate method for their addition is by (see e.g. Ref. [55]).

$$\sigma_{ppt} = \sqrt{\sigma_{ppt,1}^2 + \sigma_{ppt,2}^2} \quad (12)$$

Finally, in order to calculate the total yield strength, we also have to factor in the solid solution contribution. From the particle compositions and volume fractions, we can calculate the remaining Cu and Mg in solid solution based on the bulk composition of the alloy. As in the case of the precipitate contribution to the yield strength, the net contribution from the two solid solution alloys is expected to follow [48,55].

$$\sigma_{ss} = \sqrt{\sigma_{ss-Cu}^2 + \sigma_{ss-Mg}^2} = \sqrt{\left(k_{Cu}X_{Cu}^{2/3}\right)^2 + \left(k_{Mg}X_{Mg}^{2/3}\right)^2} \quad (13)$$

where the solid solution hardening coefficients, $k_{Cu} = 81.8$ MPa/at $\%^{2/3}$ and $k_{Mg} = 27$ MPa/at$\%^{2/3}$ are taken from Ref. [56].

Table 3 provides the various contributions from precipitates and solid solution to the overall yield strength. The relative average precipitate strength is also reported where $\beta = F_m/2\Gamma$ where $\Gamma$ is the dislocation line tension and $\beta = 1$ corresponds to the Orowan strength ($r = r_c$). To compute the total yield strength, the precipitate and solid solution contributions are summed as in Equations (13) and (12) owing to their similar magnitudes. Finally, a constant term, $\sigma_0$ , has been added to account for the effect of grain size,

$$\sigma_{ys} = \sigma_0 + \sqrt{\sigma_{ss}^2 + \sigma_{ppt}^2} \quad (14)$$

The value of $\sigma_0$ was obtained directly by measuring the yield strength of a fully solution treated sample and subtracting the solid solution contribution calculated from Equation (13).

Using the above methodology with the particle size distributions from Fig. 6 there remains only one unknown parameter($r_c$) needed to calculate the yield stress. In order to fit the yield strength measured after 20 min of aging at 200 °C (170 MPa), a value of $r_c = 3.95$ nm needs to be used. This is very close to the equivalent value ($r_c = 5$ nm) used by Deschamps et al. to describe the precipitation hardening response of an Al-1.1 at%Cu-1.7 at%Mg alloy [17].

Having established a value for $r_c$ one can test the method's ability to predict the yield stress after aging of 160 min, the results being shown in Table 3. One can see that our predicted value of the yield stress (195 MPa) is nearly identical to that measured experimentally (196 MPa). It is important to note that this good prediction would not have been possible if, in Equation (8) we would have used the mean radii of the distributions to calculate $\overline{\tau^*}$ [21]. Indeed, fitting the yield stress after 20 min of aging would require $r_c = 3.8$ nm leading to a predicted yield stress of 211 MPa in contrast to the experimental value of 196 MPa.

As noted in the introduction, the qualitative similarity of the hardening response of the low Cu alloys studied here and more conventional 2XXX series alloys has been interpreted as evidence of similar microstructural evolution on aging. Comparison of the observations presented here to those from more conventional Al-Cu-Mg alloys [15,16] suggests similarities *and* differences. In the APT observations reported in Refs. [16] and [15], following aging similar to that used here, the dominant feature of the microstructure was reported as solute clusters. Such clusters were described as roughly spherical solute enriched regions containing on average 24 solute atoms [15]. Upon aging up to peak strength (80 h at 170 °C) three different features were found to dominate; solute clusters (up to 100 atoms in size, < 4 nm in diameter), rod-like GPB zones (< 4 nm in diameter and 10–60 nm in length) and large plate like S-phase precipitates.

The features seen in Fig. 4 and quantified via the pair correlation analysis in Fig. 6 seem to situate somewhere between the features reported at short aging times and long aging times in the Al-Cu-Mg alloys noted above [15,16]. The solute clusters reported in Ref. [15] after 30 min of aging at 170 °C are similar in size and morphology to the average size of the Cu lean particles in Fig. 6 after 20 min of aging. At the longer aging times, the size of the Cu rich particles along with the tendency for more rod-like morphologies suggests a transition towards more GPB like particles, according to their definition in Ref. [16].

A significant difference between the clusters/GPB zones reported in Ref. [15] and the particles observed here are the particle chemistries. While the cluster/GPB zones in Ref. [15] were found to have Mg:Cu ratios on the order of 1.1–1.3, here the Mg:Cu ratio was found to range from as high as 16 (in the Cu lean particles at 20 min of aging) to as low as 2 (in the Cu rich particles after 160 min of aging). What is consistent with regard to chemistry across both studies, however, is that in all cases the particles are predominantly made up of Al; ~ 80 at% in this study and between ~ 85 and ~ 90 at % in Ref. [15]. The enrichment in Mg found here may not be entirely surprising considering the much higher bulk Mg:Cu ratio (14:1) for the alloy studied here compared to 0.97:1 in the alloy studied in Ref. [15]. This enrichment, combined with the high Al content of the particles, is a significant factor in the relatively high number density of particles ($N_v \approx 10^{23}$ m$^{-3}$) despite the low Cu levels employed. It is interesting to note that the behaviour seen here where small amounts of Cu can catalyze precipitation in Al-Mg alloys qualitatively mirrors the behaviour seen in Al-Cu alloys where rapid hardening is only observed when small additions of Mg are made to the alloy [16]. Indeed, the precipitation strengthening observed here is quite comparable to that reported in more conventional Al-Cu-Mg alloys despite a lower number density of particles. For example, an Al-2.5 wt%Cu-1.5 wt%Mg alloy has been reported to harden by $\Delta\sigma \approx 80$ MPa after 100–200 min of aging at 200 °C [17]. In the case of the 0.23 at%Cu alloy studied here, $\Delta\sigma = 108$ MPa evaluated after 160 min of aging at the same temperature. The strengthening potential of these clusters/GPB zones may relate to a point made in relation to strengthening in Al-Cu-Mg alloys [16] where it was argued that particles richer in Mg seemed to be more effective at hardening compared to those rich in Cu.

The ability of even very small Cu additions to efficiently catalyze the formation of a relatively high number density of predominantly

Al-Mg strengthening particles at short aging times is emphasized by the results obtained for the alloy containing only 0.12 at%Cu (Fig. 2). One can double the solutionized yield strength of both alloys studied here ($\Delta\sigma = 90$ MPa for 0.23 at.%Cu and $\Delta\sigma = 67$ MPa for 0.12 at.%Cu) by aging for 20 min at 200 °C, this despite the fact that one alloy has half as much Cu as the other. These results support those originally reported in Ref. [1] where strengthening was achieved for alloys containing as little 0.08 at%Cu. This is important given the aim of counterbalancing the ~ 25% loss in strength during the paint bake cycle [1] with the minimal addition of Cu.

Finally, we point to the significant potential for further studies focused on better understanding the precipitation sequence and kinetics in these alloys. As noted above, the nearly identical aging response at 160 °C and 200 °C is surprising. This observation suggests that there may be competing mechanisms leading to an optimal strengthening in this temperature range. Indeed, tests performed at lower temperature (100 °C, not shown here) show lower strength for the same aging time. The competition between the kinetics of excess vacancy annihilation and vacancy trapping by solute clusters may be a fruitful area for further exploration in regards to this phenomenon [57]. The observed linear dependence of yield strength on logarithmic time also warrants further study. As noted above, this behaviour is not unique to the work reported here but has also been reported by both Court and Lloyd [1] and Ratchev et al. [2]. It was suggested that the lack of variation in volume fraction of clusters/GPB zones on aging at 200 °C is most coherent with an interpretation of particle coarsening. Further to this point, if one were to adopt a simple model for coarsening kinetics see e.g. Ref. [58] then one would expect an aging response that was nearly linear in log time and whose slope would be independent of aging temperature and composition. To be able to confidently confirm or deny this interpretation would require many further studies on other alloys and other aging temperatures.

## 5. Summary

It has been shown that additions of as little as 0.12 at.%Cu to a binary Al-Mg alloy can lead to significant precipitation hardening, the observed precipitates being similar in size and chemistry to clusters/GPB zones previously reported in more conventional 2XXX-series alloys and model Al-Cu-Mg alloys. Using data extracted directly from APT measurements, the size distribution of particles could be used to predict the yield strength after aging 160 min at 200 °C following calibration of the shearable/non-shearable radius from data collected after 20 min of aging. While the strengthening particles share similar size and geometry to clusters/GPB zones in higher Cu/lower Mg alloys [15], the chemistry of the particles observed here were much leaner in Cu. This observation helps explain the relatively large number density of clusters/GPB zones despite the low bulk Cu content. Given the appreciable strengthening observed in these low Cu alloys, precipitation hardening in alloys containing very low Cu contents should be able to readily compensate for recovery induced softening in the industrial paint bake cycle. The question of the effectiveness of precipitation hardening in pre-deformed alloys, however, is the subject of ongoing work.

## Acknowledgements

U. Tezins and A. Sturm are acknowledged for their support and the running of the APT and FIB facility at MPIE. H. Zhao acknowledges the Chinese Scholarship Council for her PhD scholarship. S. Medrano acknowledges the Mexican National Council of Science and Technology (CONACyT) for his PhD scholarship. C. W. Sinclair and S. Medrano acknowledge the Natural Sciences and Engineering Research Council of Canada for financial support. Finally Novelis Inc. is thanked for the provision of materials.

## References

[1] S. Court, K. Hicklin, D.J. Lloyd, The ageing and thermal recovery behaviour of Al-Mg-Cu alloys, Mater. Sci. Forum 396–402 (2002) 1031–1036, https://doi.org/10.4028/www.scientific.net/MSF.396-402.1031. http://www.scientific.net/MSF.396-402.1031.

[2] P. Ratchev, B. Verlinden, P.D. Smet, P.V. Houtte, Artificial ageing of Al-Mg-Cu alloys, Mater. Trans., JIM 40 (1) (1999) 34–41, https://doi.org/10.2320/matertrans1989.40.34.

[3] O. Engler, C.D. Marioara, T. Hentschel, H.-J. Brinkman, Influence of copper additions on materials properties and corrosion behaviour of AlMg alloy sheet, J. Alloy. Comp. 710 (2017) 650–662, https://doi.org/10.1016/j.jallcom.2017.03.298. http://www.sciencedirect.com/science/article/pii/S0925838817311003.

[4] S.K. Das, Emerging trends in aluminum recycling, in: J.A.S. Green (Ed.), Aluminum Recycling and Processing for Energy Conservation and Sustainability, ASM International, 2007, in: http://app.knovel.com/hotlink/toc/id:kpARPECS0A/aluminum-recycling-processing/aluminum-recycling-processing.

[5] L. Kovarik, P.I. Gouma, C. Kisielowski, S.A. Court, M.J. Mills, A HRTEM study of metastable phase formation in AlMgCu alloys during artificial aging, Acta Mater. 52 (9) (2004) 2509–2520, https://doi.org/10.1016/j.actamat.2004.01.041. http://www.sciencedirect.com/science/article/pii/S1359645404000758.

[6] L. Kovarik, P.I. Gouma, C. Kisielowski, S.A. Court, M.J. Mills, Decomposition of an AlMgCu alloya high resolution transmission electron microscopy investigation, Mater. Sci. Eng., A 387389 (2004) 326–330, https://doi.org/10.1016/j.msea.2004.03.087. http://www.sciencedirect.com/science/article/pii/S092150930400499X.

[7] P. Ratchev, B. Verlinden, P. De Smet, P. Van Houtte, Precipitation hardening of an Al4.2 wt% Mg0.6 wt% Cu alloy, Acta Materialia 46 (10) (1998) 3523–3533. http://www.sciencedirect.com/science/article/pii/S1359645498000330.

[8] O. Novelo-Peralta, G. Gonzalez, G.A. Lara-Rodriguez, Characterization of precipitation in Al-Mg-Cu alloys by X-ray diffraction peak broadening analysis, Mater. Char. 59 (6) (2008) 773–780, https://doi.org/10.1016/j.matchar.2007.06.012. http://www.sciencedirect.com/science/article/pii/S1044580307002458.

[9] S.P. Ringer, K. Hono, I.J. Polmear, T. Sakurai, Precipitation processes during the early stages of ageing in Al-Cu-Mg alloys, Appl. Surf. Sci. 94–95 (1996) 253–260, https://doi.org/10.1016/0169-4332(95)00383-5. http://www.sciencedirect.com/science/article/pii/0169433295003835.

[10] S.P. Ringer, T. Sakurai, I.J. Polmear, Origins of hardening in aged Al-Cu-Mg-(Ag) alloys, Acta Mater. 45 (9) (1997) 3731–3744, https://doi.org/10.1016/S1359-6454(97)00039-6. http://www.sciencedirect.com/science/article/pii/S1359645497000396.

[11] S.P. Ringer, S.K. Caraher, I.J. Polmear, Response to comments on cluster hardening in an aged Al-Cu-Mg alloy, Scripta Mater. 39 (11) (1998) 1559–1567, https://doi.org/10.1016/S1359-6462(98)00364-9. http://www.sciencedirect.com/science/article/pii/S1359646298003649.

[12] L. Reich, S. Ringer, K. Hono, Origin of the initial rapid age hardening in an Al-1.7 at.% Mg-1.1 at.% Cu alloy, Phil. Mag. Lett. 79 (9) (1999) 639–648, https://doi.org/10.1080/095008399176689. https://doi.org/10.1080/095008399176689.

[13] A. Charai, T. Walther, C. Alfonso, A.M. Zahra, C.Y. Zahra, Coexistence of clusters, GPB zones, S-, S- and S-phases in an Al0.9% Cu1.4% Mg alloy, Acta Mater. 48 (10) (2000) 2751–2764, https://doi.org/10.1016/S1359-6454(99)00422-X. http://www.sciencedirect.com/science/article/pii/S135964549900422X.

[14] M. Starink, N. Gao, J. Yan, The origins of room temperature hardening of AlCuMg alloys, Mater. Sci. Eng., A 387–389 (2004) 222–226, https://doi.org/10.1016/j.msea.2004.01.085. http://linkinghub.elsevier.com/retrieve/pii/S0921509304005040.

[15] G. Sha, R. Marceau, X. Gao, B. Muddle, S. Ringer, Nanostructure of aluminium alloy 2024: segregation, clustering and precipitation processes, Acta Mater. 59 (4) (2011) 1659–1670, https://doi.org/10.1016/j.actamat.2010.11.033. http://linkinghub.elsevier.com/retrieve/pii/S1359645410007883.

[16] R. Marceau, G. Sha, R. Ferragut, A. Dupasquier, S. Ringer, Solute clustering in AlCuMg alloys during the early stages of elevated temperature ageing, Acta Mater. 58 (15) (2010) 4923–4939, https://doi.org/10.1016/j.actamat.2010.05.020. http://linkinghub.elsevier.com/retrieve/pii/S1359645410002958.

[17] A. Deschamps, T. Bastow, F. de Geuser, A. Hill, C. Hutchinson, In situ evaluation of the microstructure evolution during rapid hardening of an Al2.5cu1.5mg (wt.%) alloy, Acta Mater. 59 (8) (2011) 2918–2927, https://doi.org/10.1016/j.actamat.2011.01.027. http://linkinghub.elsevier.com/retrieve/pii/S1359645411000334.

[18] L. Kovarik, M.J. Mills, Structural relationship between one-dimensional crystals of GuinierPrestonBagaryatsky zones in AlCuMg alloys, Scripta Mater. 64 (11) (2011) 999–1002, https://doi.org/10.1016/j.scriptamat.2011.01.033. http://www.sciencedirect.com/science/article/pii/S1359646211000443.

[19] L. Kovarik, M.J. Mills, Ab initio analysis of GuinierPrestonBagaryatsky zone nucleation in AlCuMg alloys, Acta Mater. 60 (9) (2012) 3861–3872, https://

doi.org/10.1016/j.actamat.2012.03.044. http://www.sciencedirect.com/science/article/pii/S1359645412002340.
[20] L. Kovarik, S. Court, H. Fraser, M. Mills, GPB zones and composite GPB/GPBII zones in AlCuMg alloys, Acta Mater. 56 (17) (2008) 4804–4815, https://doi.org/10.1016/j.actamat.2008.05.042. http://linkinghub.elsevier.com/retrieve/pii/S1359645408004047.
[21] F. Fazeli, W.J. Poole, C.W. Sinclair, Modeling the effect of Al3sc precipitates on the yield stress and work hardening of an AlMgSc alloy, Acta Mater. 56 (9) (2008) 1909–1918, https://doi.org/10.1016/j.actamat.2007.12.039. http://www.sciencedirect.com/science/article/pii/S1359645407008403.
[22] B. Raeisinia, W.J. Poole, Electrical resistivity measurements: a sensitive tool for studying aluminium alloys, Mater. Sci. Forum 519–521 (2006) 1391–1396, https://doi.org/10.4028/www.scientific.net/MSF.519-521.1391. http://www.scientific.net/MSF.519-521.1391.
[23] M.K. Miller, Atom Probe Tomography, Springer US, Boston, MA, 2000, https://doi.org/10.1007/978-1-4615-4281-0. http://link.springer.com/10.1007/978-1-4615-4281-0.
[24] B. Gault, F. d. Geuser, L.T. Stephenson, M.P. Moody, B.C. Muddle, S.P. Ringer, Estimation of the reconstruction parameters for atom probe tomography, Microsc. Microanal. 14 (4) (2008) 296–305, https://doi.org/10.1017/S1431927608080690. https://www.cambridge.org/core/journals/microscopy-and-microanalysis/article/estimation-of-the-reconstruction-parameters-for-atom-probe-tomography/F989B3841A499A92314D20A72AADB16B.
[25] B. Gault, M.P. Moody, F. de Geuser, G. Tsafnat, A. La Fontaine, L.T. Stephenson, D. Haley, S.P. Ringer, Advances in the calibration of atom probe tomographic reconstruction, J. Appl. Phys. 105 (3) (2009), https://doi.org/10.1063/1.3068197, 034913, http://aip.scitation.org/doi/abs/10.1063/1.3068197.
[26] O.C. Hellman, J. B. d. Rivage, D.N. Seidman, Efficient sampling for three-dimensional atom probe microscopy data, Ultramicroscopy 95 (Supplement C) (2003) 199–205, https://doi.org/10.1016/S0304-3991(02)00317-0. http://www.sciencedirect.com/science/article/pii/S0304399102003170.
[27] U.F. Kocks, H. Mecking, Physics and phenomenology of strain hardening: the FCC case, Prog. Mater. Sci. 48 (3) (2003) 171–273, https://doi.org/10.1016/S0079-6425(02)00003-8. http://www.sciencedirect.com/science/article/pii/S0079642502000038.
[28] Alexis Deschamps, Analytical techniques for aluminum, in: Handbook of Aluminum, CRC Press, 2003. https://doi.org/10.1201/9780203912607.ch5.
[29] B. Raeisinia, W.J. Poole, D.J. Lloyd, Examination of precipitation in the aluminum alloy AA6111 using electrical resistivity measurements, Mater. Sci. Eng., A 420 (12) (2006) 245–249, https://doi.org/10.1016/j.msea.2006.01.042. http://www.sciencedirect.com/science/article/pii/S0921509306001201.
[30] S. Esmaeili, D. Vaumousse, M.W. Zandbergen, W.J. Poole, A. Cerezo, D.J. Lloyd, A study on the early-stage decomposition in the AlMgSiCu alloy AA6111 by electrical resistivity and three-dimensional atom probe, Phil. Mag. 87 (25) (2007) 3797–3816, https://doi.org/10.1080/14786430701408312. https://doi.org/10.1080/14786430701408312.
[31] A.J. Hillel, P.L. Rossiter, Resistivity mechanisms during clustering in alloys, Phil. Mag. B 44 (3) (1981) 383–388, https://doi.org/10.1080/01418638108223560. https://doi.org/10.1080/01418638108223560.
[32] M. Rosen, E. Horowitz, L. Swartzendruber, S. Fick, R. Mehrabian, The aging process in aluminum alloy 2024 studied by means of eddy currents, Mater. Sci. Eng. 53 (2) (1982) 191–198, https://doi.org/10.1016/0025-5416(82)90052-0. http://www.sciencedirect.com/science/article/pii/0025541682900520.
[33] H.-C. Shih, N.-J. Ho, J.C. Huang, Precipitation behaviors in Al-Cu-Mg and 2024 aluminum alloys, Metall. Mater. Trans. 27 (9) (1996) 2479–2494. http://link.springer.com/article/10.1007/BF02652342.
[34] B. Gault, M.P. Moody, J.M. Cairney, S.P. Ringer, Atom Probe Microscopy, Vol. 160 of Springer Series in Materials Science, Springer, New York, New York, NY, 2012, https://doi.org/10.1007/978-1-4614-3436-8. http://link.springer.com/10.1007/978-1-4614-3436-8.
[35] E.A. Marquis, J.M. Hyde, Applications of atom-probe tomography to the characterisation of solute behaviours, Mater. Sci. Eng. R Rep. 69 (4) (2010) 37–62, https://doi.org/10.1016/j.mser.2010.05.001. http://www.sciencedirect.com/science/article/pii/S0927796X10000525.
[36] R.K.W. Marceau, L.T. Stephenson, C.R. Hutchinson, S.P. Ringer, Quantitative atom probe analysis of nanostructure containing clusters and precipitates with multiple length scales, Ultramicroscopy 111 (6) (2011) 738–742, https://doi.org/10.1016/j.ultramic.2010.12.029. http://www.sciencedirect.com/science/article/pii/S0304399110003712.
[37] T. Philippe, S. Duguay, D. Blavette, Clustering and pair correlation function in atom probe tomography, Ultramicroscopy 110 (7) (2010) 862–865, https://doi.org/10.1016/j.ultramic.2010.03.004. http://www.sciencedirect.com/science/article/pii/S0304399110000823.
[38] L. Couturier, F. De Geuser, A. Deschamps, Direct comparison of Fe-Cr unmixing characterization by atom probe tomography and small angle scattering, Mater. Char. 121 (2016) 61–67, https://doi.org/10.1016/j.matchar.2016.09.028. http://www.sciencedirect.com/science/article/pii/S1044580316303333.
[39] H. Zhao, B. Gault, D. Ponge, D. Raabe, F. De Geuser, Parameter free quantitative analysis of atom probe data by correlation functions: application to the precipitation in Al-Zn-Mg-Cu, Scripta Mater. 154 (2018) 106–110, https://doi.org/10.1016/j.scriptamat.2018.05.024. https://www.sciencedirect.com/science/article/pii/S135964621830318X.
[40] R. Ivanov, A. Deschamps, F. De Geuser, A combined characterization of clusters in naturally aged AlCu(Li, Mg) alloys using small-angle neutron and X-ray scattering and atom probe tomography, J. Appl. Crystallogr. 50 (6) (2017) 1725–1734, https://doi.org/10.1107/S1600576717014443. http://onlinelibrary.wiley.com.ezproxy.library.ubc.ca/doi/10.1107/S1600576717014443/abstract.
[41] F. De Geuser, W. Lefebvre, D. Blavette, 3d atom probe study of solute atoms clustering during natural ageing and pre-ageing of an Al-Mg-Si alloy, Phil. Mag. Lett. 86 (4) (2006) 227–234, https://doi.org/10.1080/09500830600643270. http://www-tandfonline-com.ezproxy.library.ubc.ca/doi/abs/10.1080/09500830600643270.
[42] P. Debye, A.M. Bueche, Scattering by an inhomogeneous solid, J. Appl. Phys. 20 (6) (1949) 518–525, https://doi.org/10.1063/1.1698419. http://aip.scitation.org/doi/abs/10.1063/1.1698419.
[43] O. Glatter, O. Kratky (Eds.), Small Angle X-ray Scattering, Academic Press, London ; New York, 1982.
[44] A. Guinier, G. Fournet, Small-angle Scattering of X-rays, Structure of Matter, Wiley, New York, 1955.
[45] J.F. Nie, B.C. Muddle, Microstructural design of high-strength aluminum alloys, J. Phase Equil. 19 (6) (1998) 543, https://doi.org/10.1361/105497198770341734. https://link-springer-com.ezproxy.library.ubc.ca/article/10.1361/105497198770341734.
[46] K. Osamura, N. Otsuka, Y. Murakami, Resistivity maximum during Guinier-Preston zone formation in an Al-4 wt% Cu alloy, Phil. Mag. B 45 (6) (1982) 583–599, https://doi.org/10.1080/01418638208227612. http://www-tandfonline-com.ezproxy.library.ubc.ca/doi/abs/10.1080/01418638208227612.
[47] S. Hirosawa, T. Sato, J. Yokota, A. Kamio, Comparison between resistivity changes and Monte Carlo simulation for GP zone formation in Al–Cu base ternary alloys, Mater. Trans., JIM 39 (1) (1998) 139–146, https://doi.org/10.2320/matertrans1989.39.139.
[48] A. de Vaucorbeil, W.J. Poole, C.W. Sinclair, The effect of obstacle strength distribution on the critical resolved shear stress of engineering alloys, Mater. Sci. Forum 794–796 (2014) 449–454, https://doi.org/10.4028/www.scientific.net/MSF.794-796.449. https://www.scientific.net/MSF.794-796.449.
[49] A. Deschamps, Y. Brechet, Influence of predeformation and ageing of an AlZnMg alloyII. Modeling of precipitation kinetics and yield stress, Acta Mater. 47 (1) (1998) 293–305. http://www.sciencedirect.com/science/article/pii/S1359645498002961.
[50] R.K.W. Marceau, A. de Vaucorbeil, G. Sha, S.P. Ringer, W.J. Poole, Analysis of strengthening in AA6111 during the early stages of aging: atom probe tomography and yield stress modelling, Acta Mater. 61 (19) (2013) 7285–7303, https://doi.org/10.1016/j.actamat.2013.08.033. http://www.sciencedirect.com/science/article/pii/S1359645413006290.
[51] A. Baddeley, E.B.V. Jensen, Stereology for Statisticians, CRC Press, 2004.
[52] A.J. Ardell, Precipitation hardening, Metallurgical Transactions A 16 (12) (1985) 2131–2165, https://doi.org/10.1007/BF02670416. http://link.springer.com/article/10.1007/BF02670416.
[53] L. Brown, R. Ham, Dislocationparticle interactions, in: A. Kelly, R. Nicholson (Eds.), Strengthening Methods in Crystals, Elsevier Materials Science Series, John Wiley, Amsterdam, New York, 1971, pp. 12–135.
[54] A. de Vaucorbeil, C.W. Sinclair, W.J. Poole, Dislocation glide through non-randomly distributed point obstacles, Phil. Mag. 93 (27) (2013) 3664–3679, https://doi.org/10.1080/14786435.2013.820384. https://doi.org/10.1080/14786435.2013.820384.
[55] A. de Vaucorbeil, W.J. Poole, C.W. Sinclair, The superposition of strengthening contributions in engineering alloys, Mater. Sci. Eng., A 582 (2013) 147–154, https://doi.org/10.1016/j.msea.2013.06.032. http://www.sciencedirect.com/science/article/pii/S0921509313006825.
[56] O.R. Myhr, Grong, S.J. Andersen, Modelling of the age hardening behaviour of AlMgSi alloys, Acta Mater. 49 (1) (2001) 65–75, https://doi.org/10.1016/S1359-6454(00)00301-3. http://www.sciencedirect.com/science/article/pii/S1359645400003013.
[57] M.D.H. Lay, H.S. Zurob, C.R. Hutchinson, T.J. Bastow, A.J. Hill, Vacancy behavior and solute cluster growth during natural aging of an Al-Mg-Si alloy, Metall. Mater. Trans. 43 (12) (2012) 4507–4513, https://doi.org/10.1007/s11661-012-1257-7. http://link.springer.com/article/10.1007/s11661-012-1257-7.
[58] H.R. Shercliff, M.F. Ashby, A process model for age hardening of aluminium alloysI. The model, Acta Metall. Mater. 38 (10) (1990) 1789–1802, https://doi.org/10.1016/0956-7151(90)90291-N. http://www.sciencedirect.com/science/article/pii/095671519090291N.